Desalination and Water Treatment
www.deswater.com

doi:10.5004/dwt.2019.24381

160 (2019) 297–307
August

Fabrication of magnetic graphene oxide nanocomposites functionalized with a novel chelating ligand for the removal of Cr(VI): Modeling, optimization, and adsorption studies

Amir Sheikhmohammadi[a], Seyed Mohsen Mohseni[b,*], Bayram Hashemzadeh[a], Esrafil Asgari[a,*], Rahim Sharafkhani[a], Mahdieh Sardar[b], Maryam Sarkhosh[c], Mohammad Almasiane[d]

[a]*Department of Environmental Health Engineering, School of Health, Khoy University of Medical Sciences, Khoy, Iran, email: asheikh1359@gmail.com (A. Sheikhmohammadi), bayramh53@gmail.com (B. Hashemzadeh), sasgary@gmail.com (E. Asgari), r_sharafkhani@yahoo.com (R. Sharafkhani)*
[b]*Students Research Committee, Department of Environmental Health Engineering, School of Health, Shahid Beheshti University of Medical Sciences, Tehran, Iran, email: eng.mohseni.env@gmail.com (S.M. Mohseni), mahdiehsardar@yahoo.com (M. Sardar)*
[c]*Department of Environmental Health Engineering, School of Health, Mashhad University of Medical Sciences, Mashhad, Iran, email: marya.sarkhosh@yahoo.com (M. Sarkhosh)*
[d]*School of Medicine, Lorestan University of Medical Sciences, Khorramabad, Iran, email: almasian26@gmail.com (M. Almasiane)*

Received 8 December 2018; Accepted 6 May 2019

ABSTRACT

In this study, the performance of magnetic graphene oxide (GO-Fe_3O_4) functionalized with 2-mercaptobenzothiazole (MBT) chelating ligand was investigated as a new adsorbent for the adsorption of Cr(VI) from aqueous solutions. The magnetic graphene oxide functionalized with chelating ligand of the 2-mercaptobenzothiazole (GFM) was freshly synthesized via a two-stage process, and characterized by energy dispersive X-ray (EDAX), Fourier-transform infrared spectroscopy (FTIR), transmission electron microscope (TEM), scanning electron microscope (SEM) images and thermogravimetric analysis (TGA). The composition effect of independent input factors and one dependent output response was investigated using a central composite design under response surface methodology (RSM). The full second-order model indicated a model well-fitted with the experimental data. The optimum operating points giving maximum Cr(VI) removal (94.02) included pH, 6.79; adsorbent dosage, 2.98 g L^{-1}; contact time, 118.6 min; and Cr(VI) concentration, 4.41 mg L^{-1}. Based on the reported results, magnetic graphene oxide functionalized with 2-mercaptobenzothiazole (GFM) chelating ligand indicated best fit with the Langmuir model. The kinetic models followed the pseudo-first-order model. The thermodynamic studies indicated that the sorption of Cr(VI) onto GFM was endothermic and spontaneous.

Keywords: Cr(VI); Magnetic graphene oxide; 2-mercaptobenzothiazole; R software; Optimization; Modeling

1. Introduction

Hexavalent chromium (Cr(VI)) as a priority pollutant according to the US Environmental Protection Agency has received substantial attention due to its potential carcinogenicity and acute toxicity for human health, natural ecosystems, and microorganisms [1]. The Cr(VI) is widely used in many industrial processes such as metallurgical, refractories (chrome and chrome-magnesite), electroplating and metal finishing, pigment manufacturing, and tannery [2]. Cr(VI) released as a result of leakage, unsuitable storage, and improper disposal practices

*Corresponding author.

1944-3994 / 1944-3986 © 2019 Desalination Publications. All rights reserved.

can have acutely toxic effects for humans (with symptoms such as epigastria, nausea, vomiting, severe diarrhea, internal hemorrhage, dermatitis, and liver and kidney damage) [2–5]. In an aqueous environment, hexavalent chromium (Cr(VI)), such as chromate [CrO_4^{2-}, $HCrO_4^-$] is a highly mobile and soluble reactive agent (this form has the potential for increased exposure and harm to human health) and can affect biological systems. Cr(III) is not hazardous compared with Cr(VI) due to it slow solubility over a wide pH range, less mobility and much higher stability with respect to redox potential (E_h) [3,4,6–8]. Therefore,the decontamination of waters contaminated with Cr(VI) compounds before their release is an important environmental issue. Because of their simplicity, high performance, large surface areas, great adsorption capacity, presence of functional groups on their surface and also green and easy handling, nano-adsorbents (such as graphene oxide (GO)) have received much attention in wastewater treatment [9–15] and have attracted a great deal of scientific interest [4,16]. The high performance of GO in the removal of some pollutants (such as Hg^{2+} [17] and Cu^{2+} [18]) from aqueous solutions has been demonstrated by some researchers. This high performance can be due to the presence of large amounts of oxygen-containing functional groups on its surface [1]. Production of nontoxic small molecules is one of the serious effects of GO in the environment; therefore, the separation of GO from the environment is an essential issue [19,20]. Magnetic graphene oxide can be attracted by an external magnetic field, consequently solving this problem [21–23]. Magnetic adsorbents simplify the separation process, make it stronger and faster without the necessity of any additional filtration or centrifugation techniques, which resulted in the elimination of time-consuming process in the preparation of traditional adsorbents [24,25]. 2-mercaptobenzothiazole is a chelating ligand which can improve the removal performance of magnetic graphene oxide nanocomposites by creating very high metal binding capabilities [5]. So far, no specific research has been done on the application of the magnetic graphene oxide nanocomposites functionalized with 2-mercaptobenzothiazole chelating ligand in the removal of pollutants from wastewater. Therefore, for the first time, the present study introduces GFM method for Cr(VI) removal. The classical method, involving changing one parameter and fixing other parameters, is not as precise as expected and is unreliable because of its failure to describe the relationship among variables, the need for numerous tests, and being time-consuming [4,5,26]. RSM is a useful technique that can eliminate these limitations, because the effect of variables is considered simultaneously [4,27]. The R software can usefully be used for this purpose. This software can help minimize the number of required experiments, and allows specified variance criteria for estimated coefficients and estimated responses to be met [4,5]. Based on the above-mentioned facts, the present study was undertaken: (i) to optimize and find an appropriate functional relationship between the response and related input variables by RSM using R software (ii) to obtain optimum conditions of the model equation predicted by RSM using the Solver "Add-ins" (iii) and to study various isotherm models and kinetic equations to identify the possible adsorption mechanism.

2. Materials and methods

2.1. Synthesis of GO, GO-Fe_3O_4, and GFM nanocomposites

To synthesize GO and GO-Fe_3O_4, graphite powder (5 g) was mixed with 115 mL H_2SO_4 in a flask, and the mixture was stirred for 30 min. Then, $NaNO_3$ (2.5 g) was added in the flask and, to prevent agglomeration, the mixture was stirred vigorously. After that, the H_2O_2 solution (50 mL) and potassium permanganate (15 g) were added into the flask. The mixture was cooled and then was stirred for 45 min. HCl (1 mol L^{-1}) was utilized to wash the resultant suspension. To purvey the GO-Fe_3O_4 [28,29], 0.1 g of GO was mixed in 25 mL of deionized water. Then 256.5 mg $FeCl_3{\cdot}6H_2O$ and 132 mg $FeSO_4{\cdot}7H_2O$ were added in 25 mL deionized water. Then, the solution was stirred for 30 min. After that, 2 mL NH_4OH aqueous solution was added (drop by drop) into the mixture and was stirred for 4 h at 90°C under the nitrogen atmosphere. The product was washed with acetone, then separated by a magnet. The GFM nanocomposite was prepared by dispersing 1.0 g of GO-Fe_3O_4 into a flask containing 50 mL toluene, and then the mixture was stirred for 1 h. Next, 2.0 mL of 3-chloropropyl trimethoxysilane(3-CPTMS) was added into the flask and was refluxed for 12 h. An external magnetic field was applied to collect the produced black solid and the final obtained product was washed with anhydrous ethanol and was dried at 50°C. Finally, 1.0 g of the product was stirred with 50 mL of N,N′dimethylformamide and 1.0 g of 2-MBT. Then, the mixture was magnetically separated and washed with ethanol several times before drying. The schematic of the GFM nanocomposites is portrayed in Fig. 1.

2.2. Characterization of the sorbent and analytical methods

A fourier-transform infrared spectrophotometer was applied for FT-IR analysis of the products (within the range of 400–4000 cm^{-1}). The surface structural and elemental analysis of the prepared adsorbent was done by SEM (coupled with energy dispersive X-ray analysis (EDAX)) operated at an acceleration voltage of 20 kV. The thermogravimetric analysis in the temperature range of 30–800°C was applied to investigate the thermal stability of the GFM nanocomposites. The particle size of GFM was observed by using transmission electron microscopy (TEM).

2.3. Adsorption studies

Adsorption experiments were performed inside 500 mL flasks containing 200 mL Cr(VI) solutions. The stock solution of Cr(VI) ($K_2Cr_2O_7$) was made and different concentrations of chromium were prepared. A certain concentration of Cr(VI) was added into the flask. After adjusting the pH of the solution, the required dosage of the adsorbent was added inside the flask. The mixture was shaken using an orbit incubator shaker at 200 rpm for a predetermined time period. At predetermined time intervals, samples were withdrawn from the reactor and were centrifuged at 3000 rpm for 5 min. Syringe filters (0.22 μm) were applied to filter the samples extracted from the solution. To study adsorption isotherms, the mixture was shaken for 3 h at 180 rpm and environmental temperature. The equilibrium data

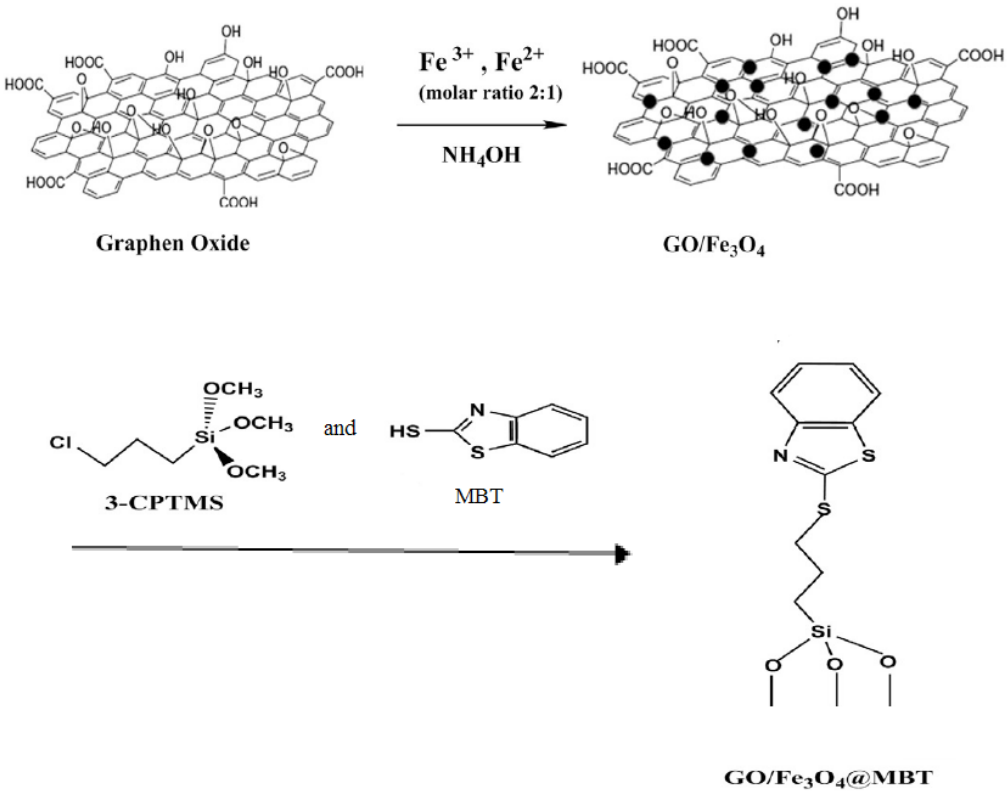

Fig. 1. The schematic representation of the synthesis of GFM.

were analyzed by the Langmuir, Freundlich, and Temkin isotherm models. Moreover, to study the adsorption kinetics, the adsorbent was added in a flask containing 200 mL of the Cr(VI) solution with a concentration of 3–9 mg L^{-1} and samples were taken at regular time intervals of 2–200 min. In this study, three types of kinetic models including pseudo-first-order, pseudo-second-order, and the Elovich models were considered. The effect of temperature on the adsorption of Cr(VI) by GFM was investigated at 288–303 K and the results of these experiments were applied to calculate the related thermodynamic parameters. Analysis of the samples were performed using a graphite furnace atomic absorption spectrometer.

2.4. Factorial experimental design and the optimization of the parameters

RSM using central composite design (CCD), as a useful statistical tool, comprises a body of methods for predicting and modeling the relationships between dependent and independent factors [27,30]. The R software for Microsoft Windows (version 3.0.3:6 March 2014) was used in order to designing the data, the generation of the three RSM models (reduced model if required), ANOVA analysis, regression analysis, designing of the final equation in terms of the uncoded factors, and description of the relationships among the dependent and independent factors by contour plots and optimization with the solver method [31]. In this research, the actual and coded values of the independent variables used for experimental design (Table 1a) and 28 runs were generated using a 4-factor central composite design with 12 center points that are presented in Table 1b (all of the specified ranges were obtained using a large number of pre-tests). Response surface was fitted using the RSM functions, including FO (first-order), TWI (two-way interaction), and SO (second-order), to specify the response-surface portion of the model [5]. The analysis of variance table was used to select the proper model [5]. Finally, the Solver "Add-ins" (using uncoded parameters, determined by regression analysis) were applied for the optimization of the selected model. The Solver is a program to write an optimization formula for a process. The data obtained in the R software are derived, and then their regression coefficients are entered into the Solver and using this process method, the optimization formula is provided for the maximum performance [30].

3. Results and discussion

3.1. Results of characterization

Detailed information about the formation of GF and GFM were obtained by FT-IR spectroscopy that are portrayed in Fig. 2. The IR spectrum of GO-Fe_3O_4 was characterized as follows (cm^{-1}): 557 cm^{-1}, 1666, 1197 and 3394 that are related to the stretching vibration of Fe-O, interaction between the carboxyl group and iron atoms (C=O), (C-O-C) and (COOH), respectively. These observations indicate the successful synthesis of GO-Fe_3O_4 (Fig. 2a). The successful modification of GO-Fe_3O_4 with MBT was proved with the

Table 1a
Actual and coded values of independent variables used for experimental design

Variable	Symbol	Coded level (GFM)		
		–1	0	1
		Real values		
pH	X_1	3	6	9
Adsorbent dose (g L^{-1})	X_2	0.5	2	3.5
Time (min)	X_3	5	62.5	120
Cr(VI) concentration (mg L^{-1})	X_4	2	6	10

Table 1b
Central composite design matrix with uncoded values of the variables

Sl. no.	Uncoded values				% Removal	
	X_1	X_2	X_3	X_4	Expt. (ϒ)	Pred. (ϒ)
1	4.5	1.25	33.75	8	20.60	18.47
2	4.5	2.75	33.75	4	69.61	71.85
3	7.5	1.25	91.25	8	40.70	52.83
4	7.5	2.75	91.25	4	83.44	93.70
5	4.5	2.75	33.75	8	56.95	62.37
6	6	2	62.50	6	68.3	72.82
7	7.5	1.25	33.75	8	17.1	24.16
8	4.5	2.75	91.25	8	73.73	78.52
9	6	2	62.50	6	76.80	72.82
10	4.5	1.25	33.75	4	22.36	27.96
11	7.5	2.75	33.75	8	69.73	68.06
12	7.5	1.25	91.25	4	55.25	62.31
13	7.5	2.75	33.75	4	71.12	77.55
14	4.5	1.25	91.25	8	43.33	47.13
15	7.5	2.75	91.25	8	76.7	84.21
16	4.5	2.75	91.25	4	76.07	88.008
17	7.5	1.25	33.75	4	36.27	33.65
18	4.5	1.25	91.25	4	54.26	56.62
19	6	2	5	6	29.63	38.33
20	6	2	62	2	71.37	70.91
21	6	2	62	6	69.78	72.82
22	6	2	62	6	64.30	72.82
23	6	2	120	6	88.4	83.14
24	6	0.5	62	6	12.5	15.09
25	6	2	62	10	49.37	51.93
26	9	2	62	6	67.8	67.66
27	3	2	62	6	52.8	56.28
28	6	3.5	62	6	92.25	90.37

presence of peaks at 2358 cm^{-1}, 2345 cm^{-1} (related to SH) and 1652 cm^{-1} (related to C=N) (Fig. 2b). SEM was used to investigate the surface morphology of GO and GFM. The results indicated an increase in the size of GFM nanocomposites in comparison with GO, proving the effective graft

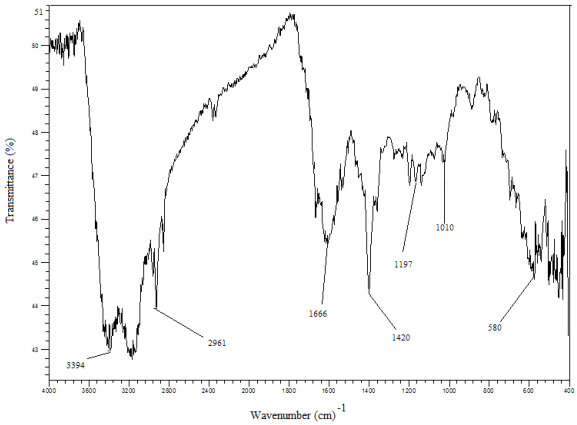

(a)

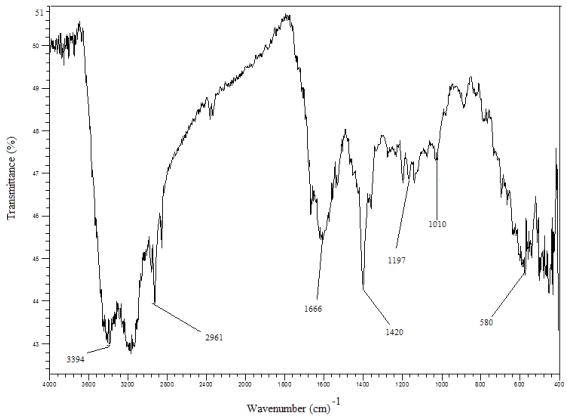

(b)

Fig. 2. The FTIR spectra for GO-Fe_3O_4 nanocomposite (a) and GFM (b).

of MBT on GO (Fig. 3. Furthermore, the results obtained from EDAX analysis indicated the presence of (Fe, C, O, N, Si and S)in the structure of GFM nanocomposites (Fig. 4a). A closer observation of TEM images with higher magnifications in Fig. 4b made the presence of ordered mesostructures clear. It can be seen that MBT anchored on GO-Fe_3O_4 and formed a large amount of GFM with different sizes. TGA analysis indicated that the nanocomposites are stable up to 600°C. The loss of residual water can be a reason for the weight reduction at 250°C. Additionally, TGA analysis proved thatGO-Fe_3O_4 loses 1.06 mg of its weight (at about 800°C). The MBT content of GFM was calculated as 13% (Fig. 5).

3.2. Response surface methodology, modeling and optimization

The three RSM models were tested to see whether they fit the data. The summary of these models is presented as information about the multiple R-squared, adjusted R-squared, F-statistic, p-value and lack of fit. The comparison of these items for the three models (FO, TWI and SO) indicated that the FO and TWI models have a lesser lack of fit, R^2 and F-value and also a greater p-value in compari-

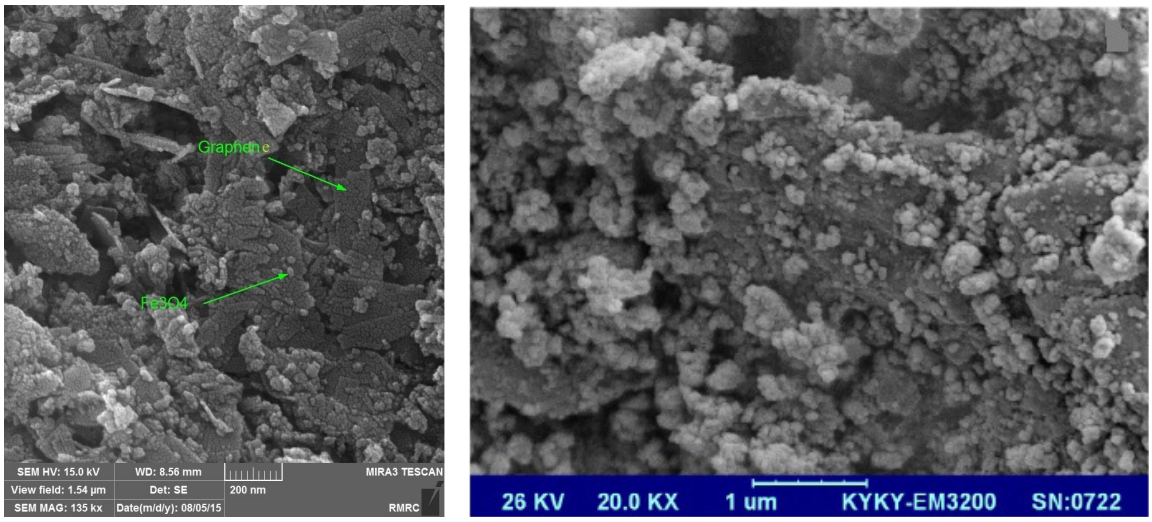

(a) (b)

Fig. 3. SEM images of GO-Fe_3O_4 (a) and GFM (b).

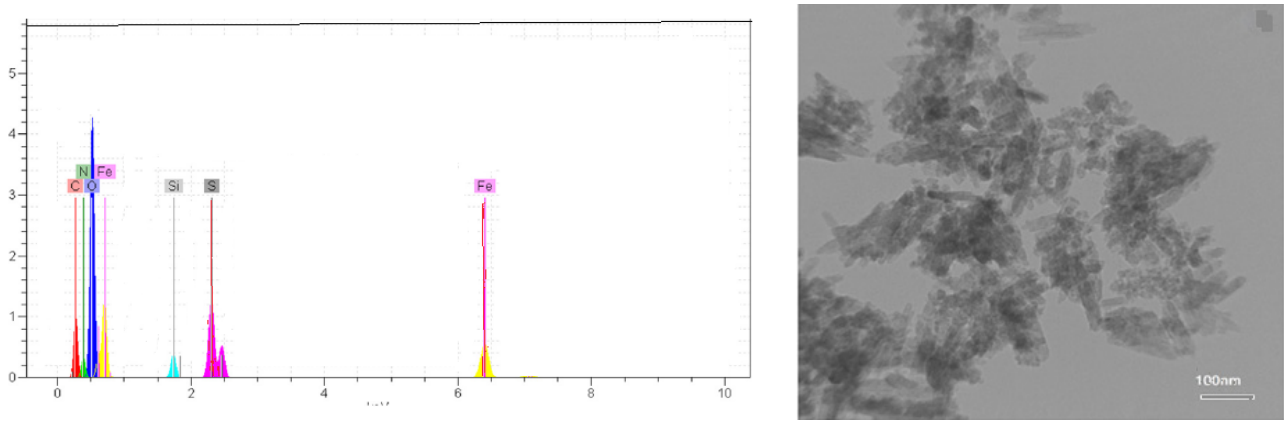

(a) (b)

Fig. 4. (a). Energy dispersive x-ray spectroscopy (EDAX) of GFM, (b). TEM image of GFM.

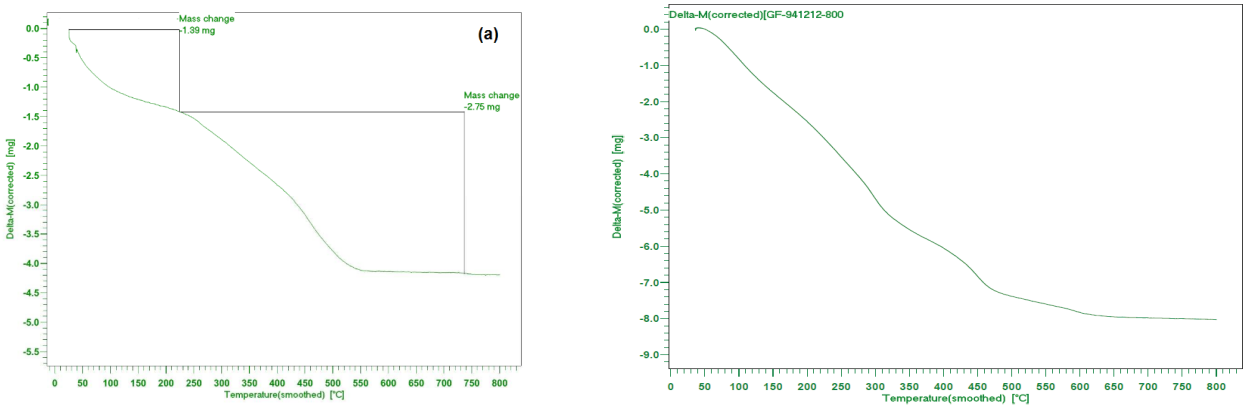

(a) (b)

Fig. 5. The TGA plots of (a) GO-Fe_3O_4 and GFM (b).

son with the SO model (Table 1a). Therefore, the SO model was selected as the best model for the prediction and optimization of GFM. Thus, ANOVA was performed for the SO model and regression coefficients were characterized. Using ANOVA, the value of the lack of fit was obtained as 0.39 (insignificant) which is appropriate for the model (Table 2b). Based on the ANOVA, the significant model formula in RSM included first-order response (X_1, X_2, X_3, X_4) and full second order response (X_1, X_2, X_3, X_4), whereas the insignificant model formula in RSM was a two-way interaction response (X_1, X_2, X_3, X_4). In addition, the regression analysis for the SO model was investigated and significant and insignificant terms were characterized (Table 2c). As Table 2c shows, the terms of the first-order response (X_1, X_2, X_3, X_4), a term of the two-way interaction response (X_2: X_3) and four terms of the pure quadratic response (X_1^2, X_2^2, X_3^2, X_4^2) were significant terms that could be entered into the model formula. Furthermore, synergistic and antagonistic effects were related to (X_1, X_2, X_3) and (X_4, X_2: X_3, X_1^2, X_2^2 , X_3^2, X_4^2), respectively. Agreement between R^2_{adj} (0.92) with R^2_{pred} (0.96) also confirmed the presence of significant terms in the model (Fig. 6).

The final equation for GFM in terms of the uncoded factors is presented below:

$$\Upsilon = -136.1 + 16.37\,X_1 + 69.8\,X_2 + 1.13\,X_3 + 6.18\,X_4 - 0.148\,X_2 X_3 - 1.2\,X_1^2 - 8.93X_2^2 - 0.0036\,X_3^2 - 0.71X_4^2 \quad (1)$$

Contour and perspective plots were used to investigate the interactive effects of variables on the performance of GFM in the removal of the Cr(VI) ions [32,33]. The interactive effects of time (20–120 min) and adsorbent dosage (0.5–3.5 g L^{-1}) on the performance of GFM are portrayed in Figs. 7a and b. As displayed in Figs. 7a and b, as time increases from 20 to 120 min, an increase in the efficiency from 20% to 70% results and thereafter it remains unchanged (at a fixed adsorbent dosage (1.5 g L^{-1})). The presence of vacant surface sites available for adsorption and the diffusion of the pollutant into the interior surface of the adsorbent have been demonstrated by the some researchers [4,34]. The researchers have stated that after a cer-

Table 2a
The comparison of different models of RSM for fitting a response-surface model

RSM models	Multiple R-squared	Adjusted R-squared	F-statistic	p-value	Lack of fit
FO	0.88	0.86	43.46 on 4 and 23 DF	2.114e-10	0.2229
TWI	0.903	0.84	15.83 on 10 and 17 DF	1.014e-06	0.1847
SO	0.962	0.92	23.67 on 14 and 13 DF	5.85e-07	0.39548

Table 2b
Analysis of variance (ANOVA) and regression analysis of the SO model for uncoded values of the variables

Model formula in RSM	DF	Sum of squares	Mean square	F-value	Probability (P)
First-order response (x_1, x_2, x_3, x_4)	4	11785.9	2946.49	76.03	6.95e-09
Two-way interaction response (x_1, x_2, x_3, x_4)	6	265	44.16	1.139	0.39340
Full second order response (x_1, x_2, x_3, x_4)	4	790.5	197.63	5.099	0.01078
Residuals	13	503.8	38.75		
Lack of fit	10	422.3	42.23	1.55	0.39548
Pure error	3	81.5	27.17		

Table 2c
Regression analysis

	Coded values				Un coded values			
Model term	Coefficient estimate	Std. error	t-value	p-value	Coefficient estimate	Std. error	t-value	p-value
(Intercept)	69.79801	3.11261	22.4243	8.926e-12	–1.361e+02	2.857e+01	–4.762	0.000156
X_1	5.28229	2.54143	2.0785	0.058034	1.637e+01	6.122e+00	2.67	0.015471
X_2	37.24694	2.54143	14.6559	1.838e-09	6.986e+01	9.179e+00	7.61	4.95e-07
X_3	21.43755	2.54143	8.4352	1.246e-06	1.137e+00	2.190e-01	5.19	6.14e-05
X_4	–9.46139	2.54143	–3.7229	0.002556	6.183e+00	3.464e+00	1.78	0.091113
X_2: X_3	–13.67075	6.22521	–2.1960	0.046838	–1.481e-01	6.469e-02	–2.29	0.034343
X_1^2	–12.03778	5.08287	–2.3683	0.034043	–1.206e+00	5.062e-01	–2.38	0.028395
X_2^2	–19.96513	5.08287	–3.9279	0.001732	–8.932e+00	2.025e+00	–4.41	0.000337
X_3^2	–13.32133	5.08287	–2.6208	0.021153	–3.657e-03	1.378e-03	–2.65	0.016146
X_4^2	–11.96513	5.08287	–2.3540	0.034964	–7.129e-01	2.847e-01	–2.50	0.022132

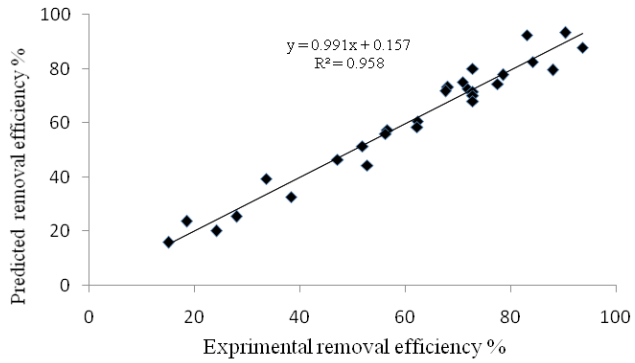

Fig. 6. Experimental Cr(VI) removal vs. predicted removal efficiency.

tain reaction time, because of the repulsive force between the adsorbent and the absorbent, the adsorbent reaches an equilibrium state that makes the remaining available surface sites difficult to occupy. Moreover, as shown in Figs. 7a and b, at a fixed initial Cr(VI) concentration of 6 mg L^{-1}, as the adsorbent dose increased from 0.5 g L^{-1} to 3.5 g L^{-1}, the adsorption efficacy increased from 13% to 86% (at a fixed time of 60 min and a pH of 6.0). This reveals that the uptake capacity of an adsorbent has a direct relationship with the adsorbent dosage. This can be attributed to the increase in the ratio of active sites/Cr(VI) consequent to increases in the GFM dosage, which can result from an increased tendency of the surface to absorb Cr(VI) ions and also be caused by the high capacity of GFM for the diffusion of the Cr(VI) into the bulk of the adsorbent. Of course, it should be noted that, in higher adsorbent doses, there is a drop in adsorbent performance that can be due to the aggregation of available binding sites [5,27,35]. The stationary points in the original units can be clear evidence of a nearby set of optimal conditions and estimate some confirmatory data near the optimum conditions. Therefore, to make sure, confirmatory data should aggregate near these points. The stationary points in the analysis of SO included pH = 7.19, adsorbent dose = 3.19 g L^{-1}, time = 87.45 min, and Cr(VI) concentration = 5.03 mg L^{-1}. The optimum conditions for the SO model were determined by the Solver "Add-ins" in Excel. The values of the entered parameters in the solver software were approximately equal to the stationary point data [4,30,36]. By simultaneously including all parameters and entering the regression coefficients of the uncoded model in the solver software, the maximum removal performance was estimated as 94.02%.The optimum conditions for the SO model at maximum removal efficiency (estimated by the Solver "Add-ins") were pH = 6.79, adsorbent dose = 2.98 g L^{-1}, time = 118.6 min, and Cr(VI) concentration = 4.41 mg L^{-1}.

3.3. Isotherm studies

Equilibrium studies were carried out under favorable conditions obtained from the model. To attain maximum sorption, the mixture was shaken for 3 h at 180 rpm and environmental temperature. The equilibrium data were analyzed using the Langmuir, Freundlich, and Temkin isotherm models. The nonlinear formulas applied for the isotherm models are tabulated in Table 3 (a). For a favorable adsorption, the value of n should be in the range of 1–10. Table 6 presents the

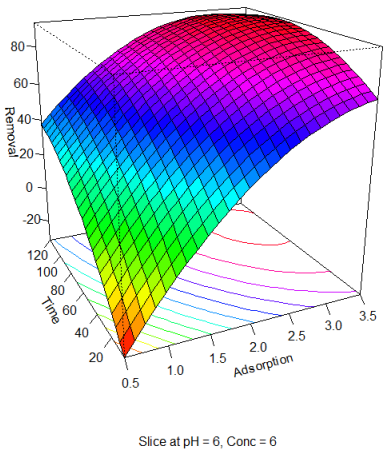

(a)

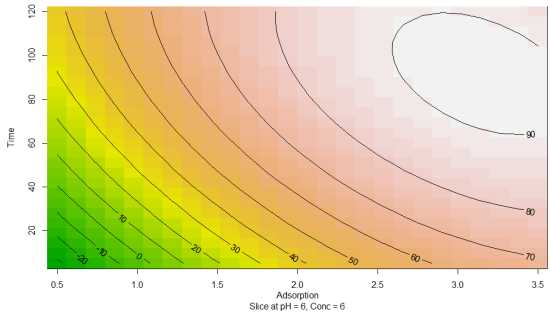

(b)

Fig. 7. Prespective (a) and contour (b) plots for the effect of adsorbent dosage and time.

parameters of the three isotherm models, including the Langmuir (a homogenous surface energy distribution), Freundlich (heterogeneous systems), and Temkin (for heterogeneous surface adsorption), showing an accurate fit of the equilibrium data. As presented in Table 3b, the Langmuir model revealed a higher correlation coefficient (R^2) than that of the rest of the isotherms. It implies that the GFM adsorbent has homogenous surface energy distribution behavior and the adsorbent layers are uniform. This means that the adsorption of a molecule to a given site is not dependent on the neighboring sites. The maximum capacity (q_m) of GFM for the adsorption of Cr(VI) was achieved at 100 mg g^{-1} (at the minimum energy 0.00006 L mg^{-1}). The maximum sorption capacities of some recently used adsorbents in the removal of Cr(VI) are presented in Table 3c. As Table 3c shows, the adsorbent used in the present study showed higher sorption capacity than that of the rest. The values of the Langmuir constant (b) indicated good affinity between the sorbent and sorbate. According to Table 3b, R_L = 0.01 and n = 3.09 (as determined by the Freundlich model), which shows that the adsorption of Cr(VI) onto GFM was favorable. The stronger adsorption ability of Cr(VI) by GFM was proved with the value of K_F =1.69 $mg^{1-1/n}/L^{1/n}/g$. The very weak bonding of Cr(VI) to the natural medium surface of the adsorbent and the slow sorption of Cr(VI) at the initial stage are reasons for the low binding constant (k_t) and the value of the adsorption heat (b_1), respectively.

Table 3a
Isotherm, kinetic and thermodynamic formula [25,38,39]

Isotherm models	Formula	Kinetic models	Formula	Thermodynamic	Formula
Langmuir	$q_e = \frac{(q_m b C_e)}{(1+bC_e)}$	Pseudo-first order	$q_t = q_e(1-e^{-k_1 t})$	Arrhenius equation	$\ln k_d = \ln A_o - \frac{E_a}{RT}$
Freundlich	$q_e = k_f C_e^{1/n}$	Pseudo-second order	$q_t = \frac{k_2 q_e^2 t}{1+k_2 q_e t}$	Enthalpy and entropy	$\ln k_d = \frac{\Delta S^\circ}{R} - \frac{\Delta H^\circ}{RT}$
Temkin	$q_e = \frac{RT}{b_1}\ln(k_t C_e)$	Elovich	$qt = \left(\frac{1}{\beta}\right)\ln(\alpha\beta) + \left(\frac{1}{\beta}\right)\ln t$	Gibbs free energy	$\Delta G^\circ = -RT\ln K_d$

where q_e (mg g^{-1}), C_e (mg L^{-1}), q_m (mg g^{-1}), b (L mg^{-1}), C_0 (mg L^{-1}), K_f (mg$^{1-1/n}$/L$^{1/n}$/g), b_1(kJ mol^{-1}), and k_t(L g^{-1}), q_t (mg g^{-1}), k_1(min^{-1}), k_2 (g mg^{-1} min^{-1}), α (mg g·min^{-1}), β (g mg^{-1}), A (g mol^{-1} min^{-1}), E_a (kJ mol^{-1}), R (8.314 J mol^{-1} K^{-1}), T (K), ΔH° (kJ mol^{-1}), ΔS°(kJ mol^{-1} K^{-1}) and ΔG° (kJ mol^{-1})

Table 3b
The adsorption isotherm parameters for the adsorption of Cr(VI) onto GFM

Isotherm model		
Langmuir	q_m (mg g^{-1})	100
	b (L mg^{-1})	0.00006
	R_L	0.013
	r^2	0.97
	Standard Error	0.14
Freundlich	K_f (mg$^{1-1/n}$/L$^{1/n}$/g)	1.69
	n	3.09
	r^2	0.933
	Standard Error	0.22
Temkin	k_t (L g^{-1})	0.073
	b_1	0.006
	r^2	0.963
	Standard Error	0.16

Table 3c
Maximum sorption capacity of some adsorbent for hexavalent chromium adsorption

Adsorbent	q_{max} (mg/g)	Reference
Mn impregnated-natural bone	88.65 ± 1	[40]
MnUiO-66	32.773	[41]
nitrogen-functionalized carbon	43.86	[42]
ZVI-GAM	15.70	[43]
CL-*g*-*p*AA	85.47	[44]
Manganese oxide incorporated ferric oxide nanocomposites	47.84	[45]
Nanoscale zero-valent iron (nZVI) Magnetite Corn Cob Silica	11.1	[46]
Magnetic graphene oxide functionalized by poly dimethyl diallyl ammonium chloride	95.2	[47]
GFM	100	Present study

3.4. Kinetic studies

The sorption kinetic studies in a wastewater treatment study provide information about the mechanism of sorption and the reaction pathways. Therefore, kinetic studies were conducted based on the pseudo-first-order, pseudo-second-order, and Elovich models. The non-liner formulas of these models are presented in Table 3a. Table 4a presents information about the parameters of the kinetic models. The predicted high R² values and also the approximate equality of the experimentally observed q_e (q_e, exp) values and the calculated q_e values (q_e, cal) were indicators for the selection of the appropriate model. As Table 4a demonstrates, it can be observed that in the pseudo-second-order kinetic model, (q_e, exp) was in good agreement with (q_e, cal). Also the high R² value for the pseudo-first-order kinetic model proved the applicability of the pseudo-first-order kinetic model to fit the experimental kinetic data. Therefore, the pseudo-first-order kinetic model was selected as the best model for the adsorption of Cr(VI) onto GFM. Based on the pseudo-first-order kinetic model, the adsorption of Cr(VI) onto GFM involves the sorption of one pollutant molecule onto one sorption site on the adsorbent surface [37]. The high rate constant (k_1 and k_2) for GFM is indicative of the shorter time needed to reach equilibrium. Furthermore, high R² values were obtained for the Elovich model. This reveals the chemisorption phenomena of Cr(VI) by GFM, assuming that the actual solid surfaces are energetically heterogeneous.

3.5. Thermodynamic studies

The influence of temperature on the performance of GFM in the removal of Cr(VI) was investigated in the range of 288–308 K. The Arrhenius equation was used to investigate the nature of the adsorption as Table 3a. Activation energy is an indicator for the adsorption type, which E_a has a value lower than 40 kJ/mol for physical adsorption and it is higher than 40 kJ/mol for chemisorption adsorption. Enthalpy (ΔH° (kJ mol^{-1})) and entropy (ΔS° (kJ mol^{-1} K^{-1})) are the other parameters used in the study of the thermodynamics of the adsorption process. The negative or positive standard entropy change (ΔS°) values depict a decrease or an increase in the randomness at the solid/liquid interface

Table 4a
Kinetic parameters for the Cr(VI) adsorption onto GFM with different initial Cr(VI) concentrations

C_0 (mg L^{-1})	Pseudo-first-order			
	q_e, exp. (mg g^{-1})	q_e, cal. (mg g^{-1})	k_1 (min^{-1})	R^2
3	0.58	1.28	0.018	0.956
6	1.14	3.16	0.011	0.995
9	1.5	5.74	0.013	0.994
	Pseudo-second-order			
	q_e, exp. (mg g^{-1})	q_e, cal. (mg g^{-1})	K_2 (min^{-1})	R^2
3	0.58	3.84	0.0039	0.955
6	1.14	20	0.00011	0.908
9	1.5	20	0.00011	0.972
	Elovich			
	α (*mg g*$^{-1}$ min^{-1})		β (*g mg*$^{-1}$)	R^2
3	0.81		2.04	0.909
6	0.47		0.85	0.992
9	0.39		0.49	0.984

Table 4b
Thermodynamic parameters for the present work

Studied adsorbent	Enthalpy (ΔH°) (kJ mol^{-1})	Entropy (ΔS°) (kJ mol^{-1} K^{-1})	ΔG° (kJ mol^{-1})		
			Absolute temperature, T (°K)		
			288	298	308
GFM	9.8	0.048	–4.08	–4.62	–5.05

during the sorption process, respectively. Spontaneity and non-spontaneity are determined by the negative or positive values of the ΔG°, respectively. Results of the thermodynamic study are tabulated in Table 4b. In the present research, the value of E_a was found to be 9.8 kJ mol^{-1} for GFM; therefore, the adsorption type is physical. The ΔH^o value for GFM was positive, indicating an endothermic sorption reaction (as T increases, the q_e value increases, too). The positive ΔS^o value for GFM proved an increase in the randomness of the adsorbed ions. The negative ΔG^o values (at all of the temperatures (288–308 K)) indicated the sorption of Cr(VI) was thermodynamically spontaneous.

3.6. Effect of co-existing water anions in the removal of Cr(VI) by GFM

To evaluate the practical application of GFM process in the removal of Cr(VI), it is indispensable to investigate the effect of co-existing water in aquatic systems; thus, the effect of real water matrix on the performance of GFM process was evaluated. The co-existing water anions were included chloride, bicarbonate, nitrate, fluoride and sulfate; the concentration of these anions in influent (real water matrix) and effluent (after application of GFM), were 150, 80, 45, 0.88 and 250 mg L^{-1} and 144, 73, 40, 0.84 and 234 mg L^{-1}, respectively. It was observed under selected conditions and in the presence of co-existing water anions, the percentage of removal decreased and reached from 94.02% to 89.05%.

3.7. Regeneration of GFM adsorbent

In the adsorption system, regeneration of adsorbent is a key factor economically. Therefore, in the present study, GFM adsorbent was regenerated to assess its reusability. The methanol was used to this purpose. To do so, 2.98 g L^{-1} of GFM adsorbent was add to solution containing 200 mL of Cr(VI) (C_o = 4.41 mg L^{-1}). After reaching the adsorption equilibrium, the adsorbent was separated by centrifuge and was generated by methanol with high purity (95%). GFM adsorbent was regenerated for five cycles. It was observed after 180 min contact time, the performance of removal Cr(VI) by GFM was 96% and 62% for the first and second cycles, respectively. The results showed that after 5 cycles of adsorbent regeneration, Cr(VI) removal efficiency was decreased severely, as the performance of removal after 90 and 180 min of reaction were 15 and 40%, respectively.

4. Conclusion

The second-order model due to a lesser lack of fit and higher R^2 and F-values was selected as the best model for prediction and optimization of GFM. Terms of (X_1, X_2, X_3) indicated a synergistic effect on the adsorption of Cr(VI) by GFM. The optimum operating points giving maximum Cr(VI) removal (94.02) was achieved pH, 6.79; adsorbent dosage, 2.98 g L^{-1}; contact time, 118.6 min and Cr(VI) concentration, 4.41 mg L^{-1}. The maximum removal performance in the selected conditions (calculated using the Solver software) was estimated as 94.02%. The maximum capacity (q_m) of GFM for the adsorption of Cr(VI) was 100 mg g^{-1}. It was characterized GFM adsorbent has a monolayer sorption behavior and adsorption of Cr(VI) onto GFM is based on sorption the one pollutant molecule onto one sorption site on the adsorbent surface. Thermodynamic studies indicated the sorption of Cr(VI) onto GFM was endothermic and spontaneous.

Acknowledgements

This study is based on the project done in the Khoy University of Medical Sciences. The authors would like to express their gratitude to the Khoy University of Medical Sciences for their financial support of this study (Ethical code: IR.KHOY.REC.1397.006).

References

[1] H. Abbas, T.S. Jamil, F. Hammad, Synthesis, characterization and photocatalytic activity of nano sized undoped and Ga doped $SrTi_{0.7}Fe_{0.3}O_3$ for 2, 4, 6-trichlorophenol photodegradation, JECE, 4 (2016) 2384–2393.
[2] L. Alidokht, A. Khataee, A. Reyhanitabar, S. Oustan, Reductive removal of Cr(VI) by starch-stabilized Fe^0 nanoparticles in aqueous solution, Desalination, 270 (2011) 105–110.
[3] H. Zhang, Y. Tang, D. Cai, X. Liu, X. Wang, Q. Huang, Z. Yu, Hexavalent chromium removal from aqueous solution by algal bloom residue derived activated carbon: equilibrium and kinetic studies, J. Hazard. Mater., 181 (2010) 801–808.

[4] A. Sheikhmohammadi, S.M. Mohseni, M. Sardar, M. Abtahi, S. Mahdavi, H. Keramati, Z. Dahaghin, S. Rezaei, M. Almasian, M. Sarkhosh, Application of graphene oxide modified with 8-hydroxyquinoline for the adsorption of Cr(VI) from wastewater: Optimization, kinetic, thermodynamic and equilibrium studies, J. Mol. Liq., 233 (2017) 75–88.
[5] A. Sheikhmohammadi, Z. Dahaghin, S.M. Mohseni, M. Sarkhosh, H. Azarpira, Z. Atafar, M. Abtahi, S. Rezaei, M. Sardar, H. Masoudi, The synthesis and application of the SiO_2@ Fe_3O_4@ MBT nanocomposite as a new magnetic sorbent for the adsorption of arsenate from aqueous solutions: Modeling, optimization, and adsorption studies, J. Mol. Liq., 255 (2018) 313–323.
[6] M.A. Rahman, M. Muneer, Photocatalysed degradation of two selected pesticide derivatives, dichlorvos and phosphamidon, in aqueous suspensions of titanium dioxide, Desalination, 181 (2005) 161–172.
[7] P. Wu, S. Li, L. Ju, N. Zhu, J. Wu, P. Li, Z. Dang, Mechanism of the reduction of hexavalent chromium by organo-montmorillonite supported iron nanoparticles, J. Hazard. Mater., 219 (2012) 283–288.
[8] Y.-X. Liu, D.-X. Yuan, J.-M. Yan, Q.-L. Li, T. Ouyang, Electrochemical removal of chromium from aqueous solutions using electrodes of stainless steel nets coated with single wall carbon nanotubes, J. Hazard. Mater., 186 (2011) 473–480.
[9] M.M. Areco, S. Hanela, J. Duran, M. dos Santos Afonso, Biosorption of Cu(II), Zn(II), Cd(II) and Pb(II) by dead biomasses of green alga Ulva lactuca and the development of a sustainable matrix for adsorption implementation, J. Hazard. Mater., 213 (2012) 123–132.
[10] U. Maheshwari, B. Mathesan, S. Gupta, Efficient adsorbent for simultaneous removal of Cu(II), Zn(II) and Cr(VI): kinetic, thermodynamics and mass transfer mechanism, Processs. Environ., 98 (2015) 198–210.
[11] W. Guo, X. Meng, Y. Liu, L. Ni, Z. Hu, R. Chen, M. Meng, Y. Wang, J. Han, M. Luo, Synthesis and application of 8-hydroxyquinoline modified magnetic mesoporous carbon for adsorption of multivariate metal ions from aqueous solutions, J. Ind. Eng. Chem., 21 (2015) 340–349.
[12] Q. Yuan, N. Li, Y. Chi, W. Geng, W. Yan, Y. Zhao, X. Li, B. Dong, Effect of large pore size of multifunctional mesoporous microsphere on removal of heavy metal ions, J. Hazard. Mater., 254 (2013) 157–165.
[13] M. Xu, W. Linghu, J. Hu, G. Jiang, J. Sheng, Utilization of Mg_2Al–layered double hydroxide as an effective sequestrator to trap Cu (II) ions from aqueous solution impacted by water quality parameters, J. Phys. Chem. Solids, 98 (2016) 100–106.
[14] Y. Li, G. Sheng, J. Sheng, Magnetite decorated graphene oxide for the highly efficient immobilization of Eu (III) from aqueous solution, J. Mol. Liq., 199 (2014) 474–480.
[15] A. Sarı, Ö.D. Uluozlü, M. Tüzen, Equilibrium, thermodynamic and kinetic investigations on biosorption of arsenic from aqueous solution by algae (Maugeotia genuflexa) biomass, Chem. Eng. J., 167 (2011) 155–161.
[16] J.D. Fowler, M.J. Allen, V.C. Tung, Y. Yang, R.B. Kaner, B.H. Weiller, Practical chemical sensors from chemically derived graphene, ACS Nano, 3 (2009) 301–306.
[17] V. Chandra, K.S. Kim, Highly selective adsorption of Hg^{2+} by a polypyrrole–reduced graphene oxide composite, Chem. Comm., 47 (2011) 3942–3944.
[18] S.-T. Yang, Y. Chang, H. Wang, G. Liu, S. Chen, Y. Wang, Y. Liu, A. Cao, Folding/aggregation of graphene oxide and its application in Cu^{2+} removal, J. Colloid. Interface Sci., 351 (2010) 122–127.
[19] X. Kong, R. Gao, X. He, L. Chen, Y. Zhang, Synthesis and characterization of the core–shell magnetic molecularly imprinted polymers (Fe_3O_4@ MIPs) adsorbents for effective extraction and determination of sulfonamides in the poultry feed, J. Chromatogr. A, 1245 (2012) 8–16.
[20] S. Xuan, F. Wang, Y.-X.J. Wang, C.Y. Jimmy, K.C.-F. Leung, Facile synthesis of size-controllable monodispersed ferrite nanospheres, J. Mater. Chem., 20 (2010) 5086–5094.
[21] L. Shao, Z. Ren, G. Zhang, L. Chen, Facile synthesis, characterization of a $MnFe_2O_4$/activated carbon magnetic composite and its effectiveness in tetracycline removal, Mater. Chem. Phys., 135 (2012) 16–24.
[22] M. Baikousi, A.B. Bourlinos, A. Douvalis, T. Bakas, D.F. Anagnostopoulos, J.i. Tuček, K.r. Šafářŏvá, R. Zboril, M.A. Karakassides, Synthesis and characterization of γ-Fe_2O_3/carbon hybrids and their application in removal of hexavalent chromium ions from aqueous solutions, Langmuir, 28 (2012) 3918–3930.
[23] Z. Wu, W. Li, P.A. Webley, D. Zhao, General and controllable synthesis of novel mesoporous magnetic iron oxide@ carbon encapsulates for efficient arsenic removal, Adv. Mater., 24 (2012) 485–491.
[24] M. Moazzen, A.M. Khaneghah, N. Shariatifar, M. Ahmadloo, I. Eş, A.N. Baghani, S. Yousefinejad, M. Alimohammadi, A. Azari, S. Dobaradaran, Multi-walled carbon nanotubes modified with iron oxide and silver nanoparticles (MWCNT-Fe_3O_4/Ag) as a novel adsorbent for determining PAEs in carbonated soft drinks using magnetic SPE-GC/MS method, Arab J. Chem., (2018).
[25] A. Kiani, M. Ahmadloo, N. Shariatifar, M. Moazzen, A.N. Baghani, G.J. Khaniki, A. Taghinezhad, A. Kouhpayeh, A.M. Khaneghah, P. Ghajarbeygi, Method development for determination of migrated phthalate acid esters from polyethylene terephthalate (PET) packaging into traditional Iranian drinking beverage (Doogh) samples: a novel approach of MSPE-GC/MS technique, Environ. Sci. Pollut. R, (2018) 1–11.
[26] J.-P. Wang, Y.-Z. Chen, Y. Wang, S.-J. Yuan, H.-Q. Yu, Optimization of the coagulation-flocculation process for pulp mill wastewater treatment using a combination of uniform design and response surface methodology, Water Res., 45 (2011) 5633–5640.
[27] A.M. Bandpei, S.M. Mohseni, A. Sheikhmohammadi, M. Sardar, M. Sarkhosh, M. Almasian, M. Avazpour, Z. Mosallanejad, Z. Atafar, S. Nazari, Optimization of arsenite removal by adsorption onto organically modified montmorillonite clay: Experimental & theoretical approaches, Korean J. Chem. Eng., 34 (2017) 376–383.
[28] Q. Chang, S. Song, Y. Wang, J. Li, J. Ma, Application of graphene as a sorbent for preconcentration and determination of trace amounts of chromium (III) in water samples by flame atomic absorption spectrometry, Anal. Methods, 4 (2012) 1110–1116.
[29] D. Li, M.B. Mueller, S. Gilje, R.B. Kaner, G.G. Wallace, Processable aqueous dispersions of graphene nanosheets, Nat. Nanotechnol, 3 (2008) 101–105.
[30] A. Mohammadi, S. Nemati, M. Mosaferi, A. Abdollahnejhad, M. Almasian, A. Sheikhmohammadi, Predicting the capability of carboxymethyl cellulose-stabilized iron nanoparticles for the remediation of arsenite from water using the response surface methodology (RSM) model: Modeling and optimization, J. Contam. Hydrol., 203 (2017) 85–92.
[31] D.C. Montgomery, Design and analysis of experiments, John wiley & sons, 2017.
[32] X. Wang, Q. Fan, S. Yu, Z. Chen, Y. Ai, Y. Sun, A. Hobiny, A. Alsaedi, X. Wang, High sorption of U (VI) on graphene oxides studied by batch experimental and theoretical calculations, Chem. Eng. Sci., 287 (2016) 448–455.
[33] Y. Sun, X. Wang, C. Ding, W. Cheng, C. Chen, T. Hayat, A. Alsaedi, J. Hu, X. Wang, Direct synthesis of bacteria-derived carbonaceous nanofibers as a highly efficient material for radionuclides elimination, ACS Sustain. Chem. Eng., 4 (2016) 4608–4616.
[34] A. Mohseni-Bandpi, T.J. Al-Musawi, E. Ghahramani, M. Zarrabi, S. Mohebi, S.A. Vahed, Improvement of zeolite adsorption capacity for cephalexin by coating with magnetic Fe_3O_4 nanoparticles, J. Mol. Liq., 218 (2016) 615–624.
[35] R. Ocampo-Pérez, J. Rivera-Utrilla, J.D. Méndez-Díaz, M. Sánchez-Polo, Modeling adsorption rate of organic micropollutants present in landfill leachates onto granular activated carbon, J. Colloid Interface Sci., 385 (2012) 174–182.
[36] R.V. Lenth, Response-Surface methods in R, using rsm, J. Statistical Software, 32 (2009) 1–17.

[37] A.S. Mohammadi, M. Sardar, M. Almasian, Equilibrum and kinetic studies on the adsorption of penicillin G by chestnut shell, EEMJ, 15 (2016).
[38] I. Rostamia, A.H. Mahvib, M.H. Dehghanib, A.N. Baghania, R. Marandid, Application of nano aluminum oxide and multi-walled carbon nanotube in fluoride removal, Desalination, 1 (2017) 6.
[39] A.N. Baghani, A.H. Mahvi, M. Gholami, N. Rastkari, M. Delikhoon, One-Pot synthesis, characterization and adsorption studies of amine-functionalized magnetite nanoparticles for removal of Cr(VI) and Ni (II) ions from aqueous solution: kinetic, isotherm and thermodynamic studies, JEHSE, 14 (2016) 11.
[40] P. Mukhopadhyay, R. Chakraborty, M. Chakraborty, A. Mitra, Infrared irradiation aided fabrication of Mn impregnated-natural bone adsorbent: Efficacy evaluation in aqueous Cr(VI) removal, J. Water Process. Eng., 6 (2015) 32–41.
[41] Z.-h. Yang, J. Cao, Y.-p. Chen, X. Li, W.-p. Xiong, Y.-y. Zhou, C.-y. Zhou, R. Xu, Y.-r. Zhang, Mn-doped zirconium metal-organic framework as an effective adsorbent for removal of tetracycline and Cr(VI) from aqueous solution, Micropor.s Mesopor. Mater., (2018).
[42] Z. Guo, J. Zhang, H. Liu, Y. Kang, Development of a nitrogen-functionalized carbon adsorbent derived from biomass waste by diammonium hydrogen phosphate activation for Cr(VI) removal, Powder. Tech., 318 (2017) 459–464.
[43] J. Liu, T. Mwamulima, Y. Wang, Y. Fang, S. Song, C. Peng, Removal of Pb (II) and Cr(VI) from aqueous solutions using the fly ash-based adsorbent material-supported zero-valent iron, J. Mol. Liq., 243 (2017) 205–211.
[44] Y. Wang, B. Du, J. Wang, Y. Wang, H. Gu, X. Zhang, Synthesis and characterization of a high capacity ionic modified hydrogel adsorbent and its application in the removal of Cr(VI) from aqueous solution, JECE, 6 (2018) 6881–6890.
[45] A. Ghosh, M. Pal, K. Biswas, U.C. Ghosh, B. Manna, Manganese oxide incorporated ferric oxide nanocomposites (MIFN): A novel adsorbent for effective removal of Cr(VI) from contaminated water, J. Wat. Process. Eng., 7 (2015) 176–186.
[46] D. Kumari, R. Goswami, M. Kumar, R. Kataki, J. Shim, Removal of Cr(VI) ions from the aqueous solution through nanoscale zero-valent iron (nZVI) Magnetite Corn Cob Silica (MCCS): A bio-waste based water purification perspective, Ground. Sustain. Develop., 7 (2018) 470–476.
[47] N. Li, Q. Yue, B. Gao, X. Xu, Y. Kan, P. Zhao, Magnetic graphene oxide functionalized by poly dimethyl diallyl ammonium chloride for efficient removal of Cr(VI), J. Taiwan Inst. Chem. Eng., 91 (2018) 499–506.
[48] G. Gao, L. Nie, S. Yang, P. Jin, R. Chen, D. Ding, X.C. Wang, W. Wang, K. Wu, Q. Zhang, Well-defined strategy for development of adsorbent using metal organic frameworks (MOF) template for high performance removal of hexavalent chromium, Appl. Surf. Sci., 457 (2018) 1208–1217.